Pergamon

PII: S0301-9322(96)00088-2

Int. J. Multiphase Flow Vol. 23, No. 3, pp. 473–491, 1997

Printed in Great Britain
0301-9322/97 $17.00 + 0.00

GAS FILTRATION DURING THE IMPACT OF WEAK SHOCK WAVES ON GRANULAR LAYERS

A. BRITAN, G. BEN-DOR, T. ELPERIN, O. IGRA and J. P. JIANG

Pearlstone Center for Aeronautical Engineering Studies, Department of Mechanical Engineering, Ben-Gurion University of the Negev, P.O. Box. 653, Beer-Sheva 84105, Israel

(Received 22 August 1996; in revised form 2 December 1996)

Abstract—This paper deals with the unsteady gas filtration through a granular layer attached to a rigid end-wall when impacted head-on by a weak shock wave in a shock tube. The main goal of the present work is to study the gas pressure field developed inside the granular layer during its compression by the shock wave. A physical model is proposed for simulating the phenomenon and solved numerically. The numerical results are compared with the measured gas pressure at different locations inside the sample and at the end-wall covered by the granular layers.

Good agreement is found between the calculated gas pressure signals and those measured at the shock tube end-wall covered by a granular layer at the final stage when the gas pressure is mostly governed by gas filtration. In the initial, unsteady part of the signals, large deviations exist between the calculated and the experimental results. The only reason for the agreement or discrepancy between the theoretical predictions and the experiments is the compaction effect associated with the formation of the gas pressure profile at the shock tube end-wall covered with a granular layer. © 1997 Elsevier Science Ltd. All rights reserved.

Key Words: granular layer, shock wave, impact, permeability

1. INTRODUCTION

Unsteady filtration of shock wave induced gas flow through a granular medium is encountered in various civil and military applications. Gas filtration is a major result of the impact process. Although this phenomenon can be simulated successfully, only few numerical studies were published on this subject while the steady gas filtration through a porous medium is well documented (e.g. Dullien 1992; Molerus 1993).

The study by Gelfand *et al.* (1989) was probably the first where filtration effects were observed in shock tube experiments with granular layers of different thickness and materials. However, this study did not address the role of this effect on the formation of the compressive stress inside the layer. Sakakita and Hayashi (1992) also studied the head-on collision of a planar shock wave with a granular layer. They analyzed two different samples, both were 10 mm thick. In the theoretical part of their work the conservation equations for a dust suspension were used. In order to include the effects associated with the contact between solid particles (which is unavoidable in granular layers) new terms were added to the conservation equations. One accounts for the variations in the volume fractions of both, the solid and the gaseous phases; the other describes the stresses inside the granular layer due to the particle-particle interactions. Poor agreement was obtained between the numerical and the experimental results of the compressive stress. The effect of the gas filtration was included in their study.

A similar model was proposed by Kutushev and Rudakov (1993) for simulating the pressure signals measured by Gelfand *et al.* (1989). Kutushev and Rudakov (1993) simulated experiments for a granular layer length of $L = 20$ mm. The particles composing the layer were treated as a deformable body. A qualitative agreement was obtained between the calculated and the measured compressive stresses at the shock tube end-wall. Kutushev and Rudakov (1993) noted that changes in the gas pressure inside the granular layer were governed by the gas filtration. However, the calculated gas pressure histories at the end-wall, shown in their paper, were not compared with the experimental results. The investigation of Kutushev and Rudakov (1993) left several questions unanswered, such as the use of fitting parameters which were not known *a priori*, and the validity of the constitutive equation used in their simulation.

Rogg *et al.* (1985) assumed in their calculations that the solid particles do not move and coupled the pure gas region with the granular layer by a quasi-steady flow assumption at the gas–granular layer interface. In this way the two phase flow problem was reduced to a pure gas problem. By fitting some parameters an acceptable agreement between the experimental and the numerical results was obtained inside the layer, but not in the pure gas region.

The same approach was used by Ben-Dor *et al.* (1996) for the numerical simulations of the gas pressure history inside rigid porous samples whose porosity were about $\epsilon = 0.745$ and 0.82. Good agreement was found between the numerical simulations and the experimental results. In all the above mentioned studies, correlations obtained for a packed bed and a steady flow were used for treating the momentum and energy exchanges between the gas and the solid phases. Review of studies on momentum and energy transfer in packed beds can be found in Rogg *et al.* (1985), Dullien (1992), Molerus (1993).

Notably, most of the above mentioned studies did not address the coupling which exists between the compression of the granular medium and the gas filtration inside it. An analysis of the experimental results obtained in our previous studies (see, e.g. Britan *et al.* 1995; Ben-Dor *et al.* 1997; Britan *et al.* 1997) clearly indicates that the compaction and the gas filtration are important factors which affect the waves propagation and the compressive stress formation inside the granular medium. Moreover, in reality these phenomena influence each other and it is difficult to separate between them when analyzing experimental data.

For this purpose we performed a series of numerical calculations employing a well established and validated filtration model. The simulated gas pressure histories were compared with experimental data obtained for granular layers with different characteristics. In contrast to the studies of Rogg *et al.* (1985), Levy *et al.* (1993), Kutushev and Rudakov (1993) we did not employ any fitting parameters in the calculations and obtained results which provided a useful guide for explaining filtration effects in granular media. This study corrects the pervious assertion on the role of filtration inside materials with different characteristics. Namely, since the filtration plays a significant role in granular materials with large permeability, the compression of the sample during the impact strongly depends on the drag forces between the gas flow and the particles. In materials having small permeability the main effects in the sample compression are related to the direct transmission of the impact force through the contact points between the particles (see, e.g. Britan *et al.* 1997).

2. EXPERIMENTAL STUDY

The experimental part of this study was conducted in a small vertical shock tube described in details in Ben-Dor *et al.* (1997). The shock tube has a constant square cross-section 31 mm × 31 mm, including the driver (0.8 m long) and the channel (1.5 m long). Ambient air was used in the low pressure chamber. The driver chamber was filled with air at initial pressure 0.55 ± 0.001 MPa. The Mach number of the incident shock wave was about $M_s = 1.3$ and did not vary significantly between different experiments since the diaphragm was ruptured with the aid of a special knife when a desired pressure in the driver chamber was reached.

To improve repeatability of the initial conditions and homogeneity of the granular layers a special test section (0.14 m long) was constructed for preparation of the samples. Prior to the experiment this section was lifted off the holding flange at the rear end of the channel, and during the material filling light knocking at the test section wall was applied. Special attention was given to ensure that the granular layer free surface remained flat and normal to the side-wall. Once a preparation procedure was completed, the layer thickness L was measured with an accuracy of about ± 1 mm, and the test section with the granular material was bolted at the rear flange.

The test section (see figure 1) was instrumented with pressure transducers T1–T4 which were protected from having a direct contact with the granular material particles by a screen permeable to the gas. This was done in order to measure the local gas pressure inside the layer. A pressure transducer T5 without a screen was installed at the end-wall in order to measure the compressive stress there. The recorded data were stored using a data acquisition system sampling at 500 kHz per channel on an IBM-486 computer (for more details see Ben-Dor *et al.* 1997).

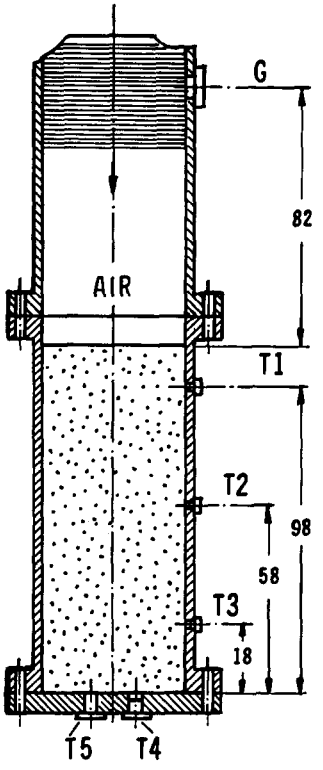

Figure 1. Schematic description of the test section of the vertical shock tube.

The parameters of the granular materials are given in table 1. The particle spatial density ρ_p, was calculated using the measured weight and volume. The mean diameter of the granules d_p, for materials N1–N3 was measured by a microscope with an accuracy of ± 0.01 mm. Powders N4 and N5 were grated using sieves with calibrated mesh sizes. The bulk densities ρ_c were determined from the overall layer volume and its weight in air. The porosity was calculated from: $\epsilon = 1 - \rho_c/\rho_p$ and for the permeability of the granular layer f the following Carman–Cozeny formula, derived for the monospherical particles, was used (see, e.g. Dullien 1992):

$$f = \frac{d_p^2}{180}\left(\frac{\epsilon_G^3}{(1-\epsilon_G)^2}\right). \qquad [1]$$

Hereafter, for convenience each tested material will be identified in the text and the figures by the code number assigned to it in table 1.

3. THEORY

3.1. *The assumptions*

Prior to the head-on collision between the incident shock wave and the granular layer the solid and the gas phases composing the layer are in a state of equilibrium. Immediately after the collision

Table 1. Characteristics of the granular materials used in the experiments

N	Material	d_p (mm)	ρ_p (g/cm^3)	ρ_c (g/cm^3)	ϵ	f (mm^2)
1	PVC	3.33	1.40	0.86	0.39	0.00954
2	Al_2O_3	1.67	0.96	0.51	0.46	0.00496
3	Fe	1.04	7.41	4.50	0.39	0.00099
4	Fe	0.45	7.41	4.46	0.40	0.00018
5	Potash	0.45	1.90	1.10	0.42	0.00027

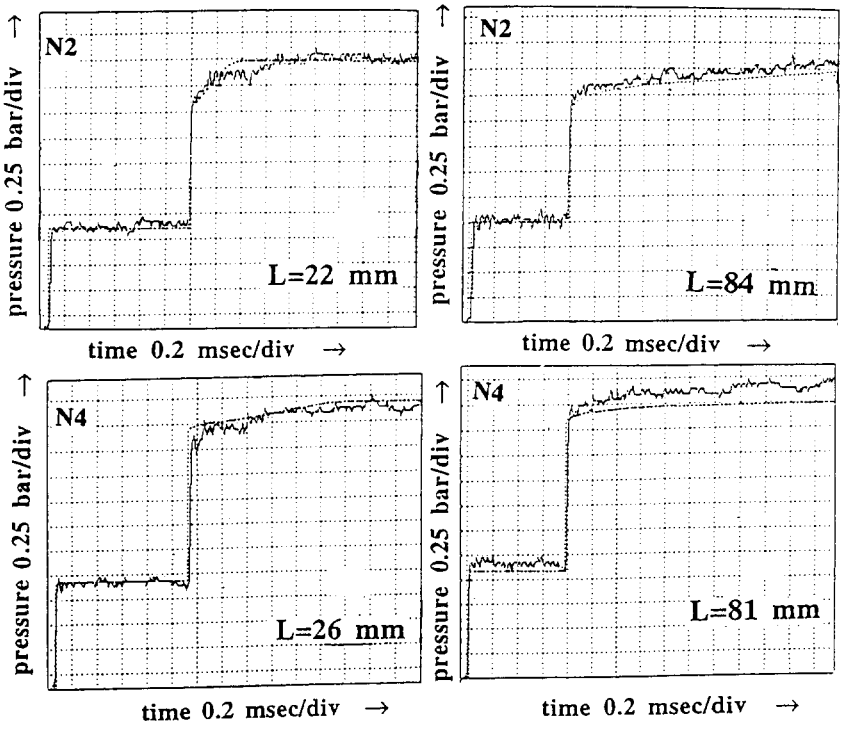

Figure 2. Typical gas pressure signals from transducer G (solid curves) and their numerical simulation (dotted line) for two types of granular layers and different depths.

intensive momentum and heat transfer between the two phases begin and the induced flow pattern inside the granular medium involves pressure waves, vortices, jets, and turbulence (Rogg *et al.* 1985). A complete study of such phenomena, either analytical or numerical, is very complicated. Hence it is important to simplify the problem in order to make it manageable while maintaining the essential and dominant features of the phenomenon. This can be done by employing the following assumptions.

(1) Both the gas and solid phases are chemically inert; the solid particles are uniformly distributed inside the granular layer.
(2) The distance over which the mean flow parameters vary significantly is much greater than the characteristic dimension of the solid particles and the distance between neighboring particles. Therefore, both the gas and the solid phases can be treated as a continuum.
(3) All the solid particles are of identical size and have spherical shape which is maintained during the impact.
(4) The stress appears in a granular medium when it is compressed; the stress vanishes when the particles are dispersed.
(5) The specific heat capacity of the solid phase is constant. The thermal gradients within the particles can be neglected because the thermal diffusivity of the solid particles is relatively high and the particles are relatively small.
(6) Only heat and momentum transfer between the solid and the gaseous phases are taken into account.
(7) The gaseous phase behaves like a perfect gas.
(8) The flow field is one-dimensional.

For a moderate shock waves ($M_s < 2$) the following further simplifying assumptions can be added:

(9) Inside the granular layer the shock wave induced gas flow velocity is low, the unsteady effects are small and a steady state approximation for the friction force can be used.

(10) The skeleton of the granular layer during the compaction is not compressed and therefore, the porosity changes are negligibly small.

The use of the two last assumptions is restricted to the case when the particles do not move and the porosity of the layer ϵ is constant. Indeed, most of the granular materials used in our experiments are quite hard (e.g. Fe, Al_2O_3). Moreover, special attention was given to prepare the sample with as high as possible packing (for more details, see Ben-Dor *et al.* 1997).

3.2. The governing equations

The mass, momentum and energy conservation equations under these assumptions can be written as:

$$\frac{\partial \rho_G}{\partial t} + \frac{\partial (\rho_G V_G)}{\partial x} = 0, \qquad [2]$$

$$\frac{\partial (\rho_G V_G)}{\partial t} + \frac{\partial (\rho_G V_G^2)}{\partial x} + \frac{\partial P_G}{\partial x} = \frac{F_G}{\epsilon_G}, \qquad [3]$$

$$\frac{\partial \left\{ \rho_G \left(c_G T_G + \frac{1}{2} V_g^2 \right) \right\}}{\partial t} + \frac{\partial \left\{ \rho_G V_G \left(c_G T_G + \frac{1}{2} V_g^2 + \frac{P_G}{\rho_G} \right) \right\}}{\partial x} = \frac{Q_G - F_G V_G}{\epsilon_G}. \qquad [4]$$

The heat conduction equation for the solid phase reads:

$$\frac{\partial T_p}{\partial t} = \frac{-Q_G + F_G V_G}{\epsilon_p \rho_p c_p}, \quad \text{for} \quad \epsilon_G \neq 1. \qquad [5]$$

To solve the system [2]–[5] we use the equation of state of a perfect gas for the gaseous phase and the following equations for the friction losses and heat transfer rates Q_G per unit volume of gas–solid mixture: (see, Kaviany 1991; Bird *et al.* 1960):

$$P_G = R_G \rho_G T_G, \qquad [6]$$

$$\frac{F_G}{\epsilon_G} = -\frac{\rho_G V_G^2}{d_p} \frac{1 - \epsilon_G}{\epsilon_G} \left[\frac{A(1 - \epsilon_G)}{\mathrm{Re}_p} + B \right], \quad \text{for} \quad \epsilon_G \neq 1, \qquad [7]$$

$$Q_G = h \frac{6(1 - \epsilon_G)}{d_p} (T_p - T_G), \quad \text{for} \quad \epsilon_G \neq 1, \qquad [8]$$

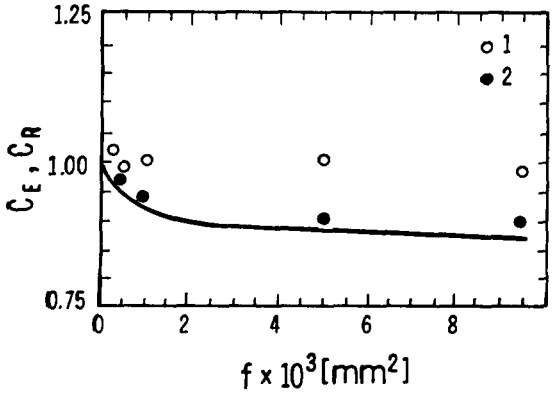

Figure 3. Measured values of the coefficients C_E: (1) and C_R: (2) vs the granular layer permeability f. Solid line-calculated relation for C_R vs f.

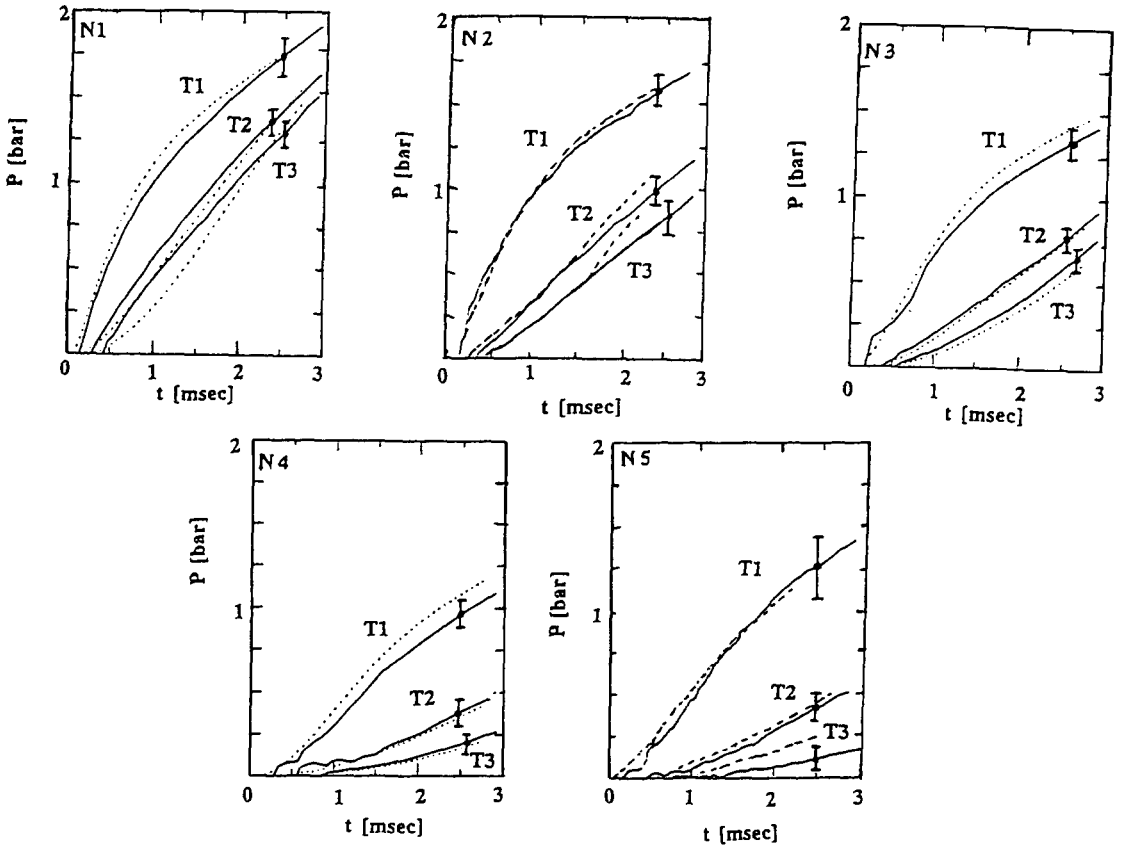

Figure 4. Comparison of the measured (solid curves) and the calculated (dotted curves) gas pressure signals from transducers T1–T3, for $L = 138$ mm.

$$h = j \cdot c_p \rho_G \epsilon_G V_G \left(\frac{c_{P_G}\mu}{k}\right)^{-2/3}, \quad [9]$$

$$j = 0.91 R_{ej}^{-0.51}, \quad \text{for} \quad R_{ej} < 50, \quad [10]$$

$$j = 0.61 R_{ej}^{-0.41}, \quad \text{for} \quad R_{ej} > 50,$$

$$Re_p = \frac{\rho_G \epsilon_G V_G d_p}{\mu}, \quad [11]$$

$$R_{ej} = \frac{\rho_G \epsilon_G V_G d_p}{6(1-\epsilon_G)\mu}, \quad [12]$$

$$\mu = 1.71 \times 10^{-5} \left(\frac{T_G}{273}\right)^{0.73}. \quad [13]$$

Here ρ_G, ϵ_G, c_G, ρ_p, ϵ_p, c_p are the material density, the porosity and the specific heat capacity at constant volume of the gas (subscript G) and of the solid phase (subscript p); T_G, V_G, e_G, T_p, V_p, e_p are the temperature, the velocity, the specific internal energy of the gas (subscript G) and the solid phase (subscript p); P_G and R_G are the gas pressure and the gas constant; P_p is the particle pressure; F_G and F_p are the body force, per unit volume of the mixture, acting on the gas (subscript G) and the particle (subscript p); d_p is the particle diameter; h is the heat-transfer coefficient; c_{PG} is the specific heat capacity at constant pressure of the gas; μ is the gas viscosity. Q_G and Q_p are the heat transfer rates, per unit volume, of the gas–solid mixture into the gas (subscript G) and

into the particle (subscript p); $k = 2.532 \times 10^{-2}$ J/msK is a coefficient of the thermal conductivity for air.

According to the theory of homogeneous mixtures (see, e.g. Ishii 1975; Gouph and Zwarts 1979; Drew 1983), the work rates, per unit volume, of the mixture done by the gas on the particle W_G and by the particle on the gas W_p can be written as:

$$W_G = -W_p = -F_G V_G, \quad Q_G = -Q_p.$$

The coefficients A and B in Ergun's equation [7] for the friction force during gas filtration are: $A = 180$ and $1.8 \leqslant B \leqslant 4.0$. For the present case we used $B = 1.8$ because the particles have smooth surfaces (Mac-Donald *et al.* 1979).

Based on calculation it was evident, that the above model is not sensitive to up to 10% changes in the porosity. This fact further supports the use of the model with a constant porosity, i.e. neglecting the compactation of the granular layer during the impact.

3.3. The numerical method

Since the system [2]–[13] cannot be solved analytically, a numerical solution was conducted. The employed numerical method should be capable of producing an accurate solution with a reasonable grid spacing. Hence, a high-order shock-capturing method was needed.

The TVD (total variation diminishing) scheme of second order accuracy in space and time was used in the present numerical computations to solve the homogeneous system [2]–[4]. It is a nonoscillatory dissipative scheme containing no free parameters with high resolution of

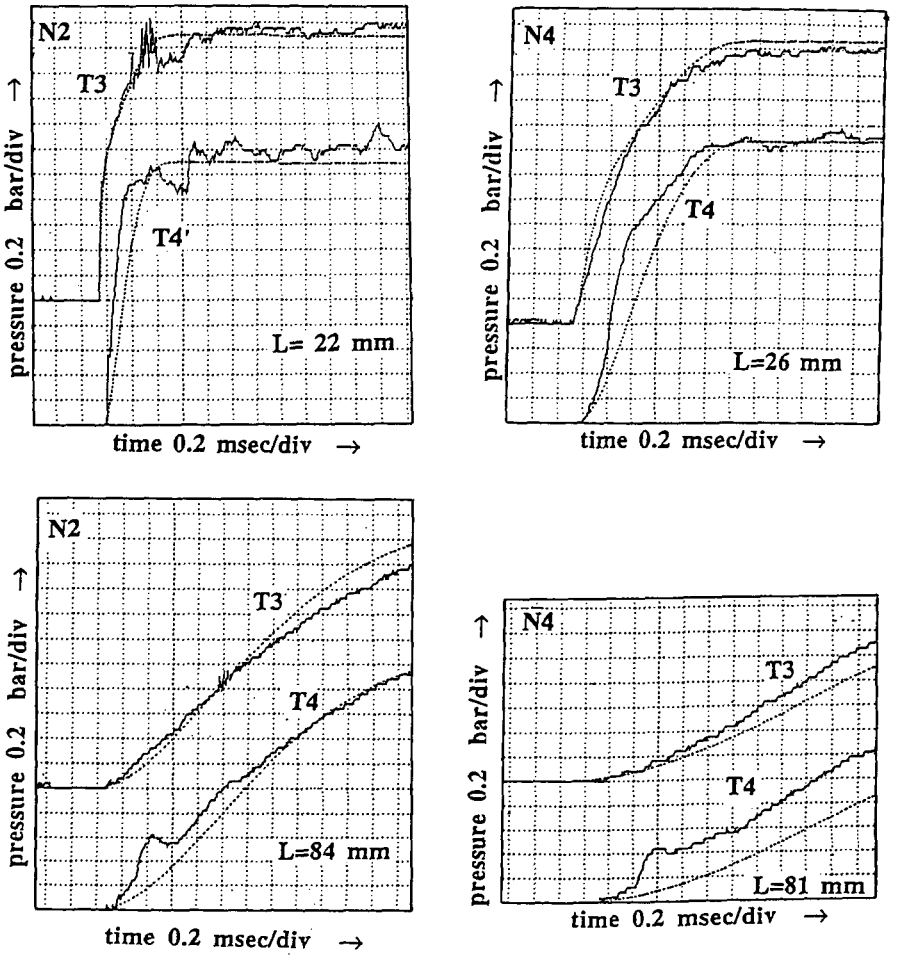

Figure 5. Comparison of the measured (solid curves) and the calculated (dotted curves) gas pressure signals from transducers T3 and T4 for two types of granular layers and different depths.

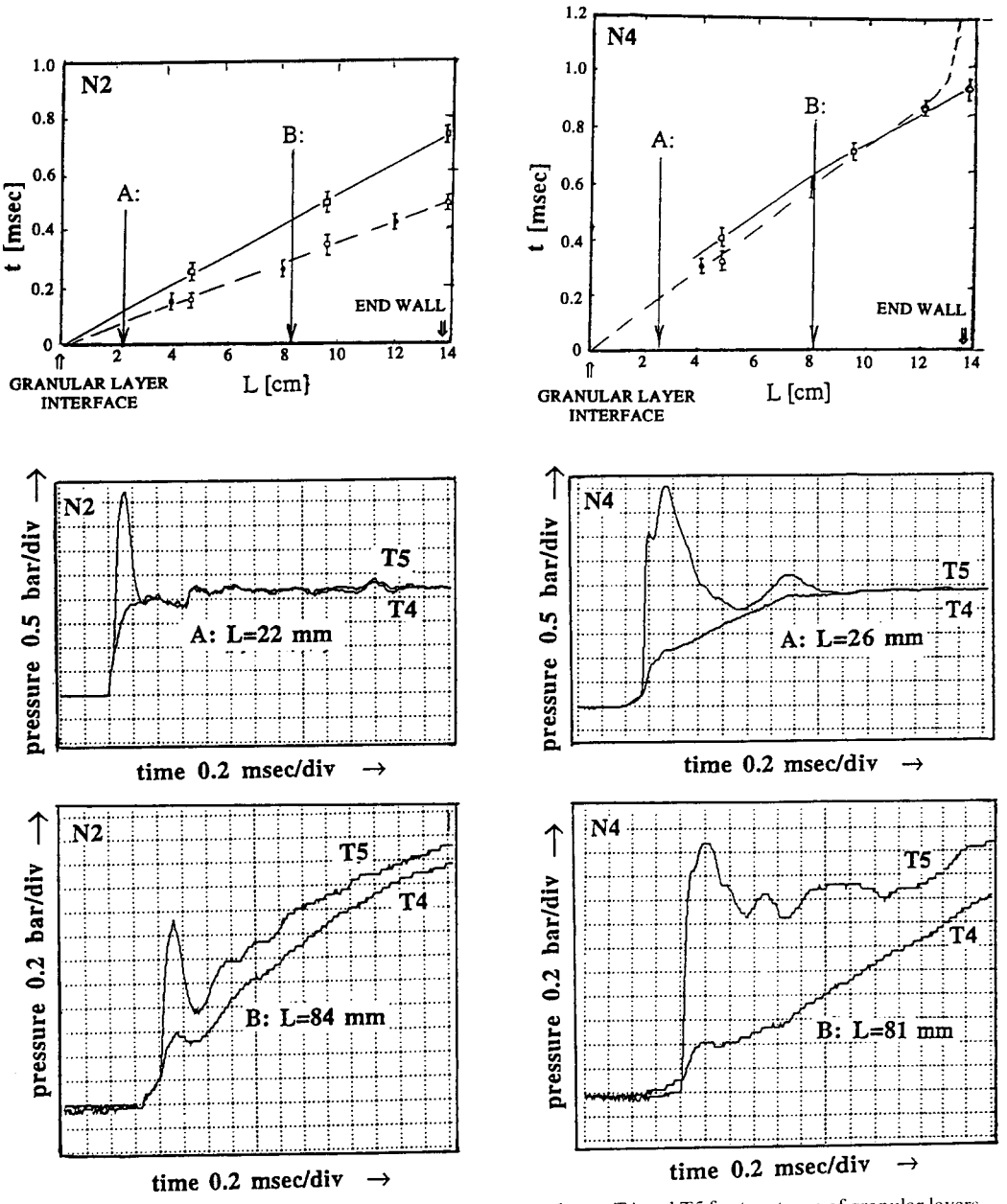

Figure 6. Wave diagrams and pressure signals from transducers T4 and T5 for two types of granular layers and different depths.

discontinuities. The source terms were treated using operator splitting techniques (for details see Hirsch 1991).

4. COMPARISON BETWEEN THE NUMERICAL AND THE EXPERIMENTAL RESULTS

The main details of the compressive stress formation inside the granular medium were discussed previously by Britan *et al.* (1995), Ben-Dor *et al.* (1997) and Britan *et al.* (1997). The present study is a continuation of these investigations, and is primarily concerned with the gas filtration effect inside the granular layer. First, computer simulated and measured results were compared for signals obtained from the side-wall transducers G, T1, T2 and T3 for granular layers depth of $L = 138$ mm. Next, the same comparison was performed for signals obtained from transducer T4, flush mounted at the end-wall and covered by granular layers of different depth L. In both cases, five kinds of the

the granular materials, listed in table 1, were studied. To verify the proposed numerical model, no adjustable parameters were used and the model parameters were the same for the different materials and lengths of the granular samples. All the computations were made for an incident shock wave having a Mach number, $M_s = 1.3$.

4.1. Gas pressure ahead of the granular layer

During the weak shock wave impact on the granular layer, the position of the interface does not change significantly, and the velocity of the shock induced flow is mainly governed by the permeability of the material. Some information of how the permeability affects the gas pressure profile behind the reflected shock wave as measured by the transducer G is presented in figure 2. The first pressure jump in these figures is due to the incident shock wave, and the second one is due to the shock wave which reflects from the air–granular layer interface. It is clear from these pressure histories that behind the reflected shock wave the gas pressure rises continuously up to

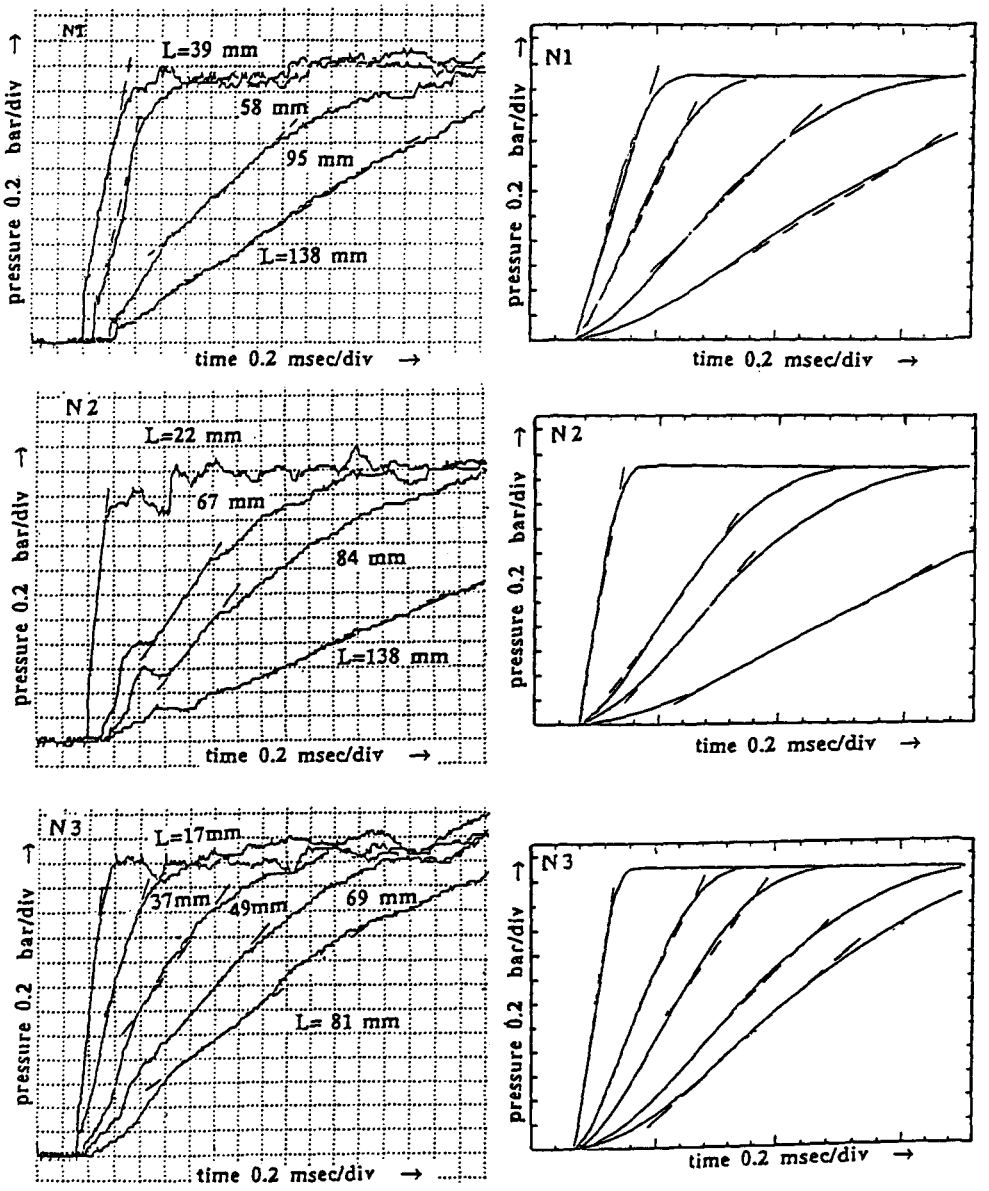

Figure 7. Typical gas pressure signals from transducer T4 (on the left) and their numerical simulation (on the right) for material N1–N3 and different sample depth. Dotted straight lines show the tangent to the linear sections of the curves.

values which would have been obtained had the incident shock wave ($M_s = 1.3$) reflected head-on from a rigid end-wall. According to Rogg *et al.* (1985) and Levy *et al.* (1993) such an effect can be related to the compression waves which emerge from the granular layer during the gas filtration through the layer which catch up with the reflected shock wave. This simple model also explains the difference between the pressure profiles as measured with the short ($L = 22$ mm) and the long ($L = 84$ mm) samples of material N2. Actually, while penetrating into the long sample the transmitted wave attenuates, and the reflected compression wave becomes more and more dispersed and causes the gradual rise of the gas pressure behind the reflected shock wave. For the short layer, a strong transmitted wave can reflect at the end-wall and reach the interface without attenuation. Thus, the effect of the compressive waves on the gas pressure registered by the transducer G is more pronounced. Notably, the calculated profiles of the gas pressure shown by the dotted lines in figure 2 agree quite well with the experimental results. Although figure 2 describes the results of only four experiments and calculations, similar data were obtained for all the studied conditions. As can be seen from the data in figure 2 the effect of the permeability is similar to that of the sample length, *viz.*, the less is the permeability of the layer or the larger is the sample depth L, the smoother is the pressure profile behind the reflected shock wave.

In order to describe this unsteady profile we introduce a reflection coefficients:

$$C_R = \frac{P_R - P_2}{P_6 - P_2} \quad \text{and} \quad C_E = P_e/P_6,$$

where P_R is the magnitude of the first pressure jump, P_e is the maximum quasi steady pressure behind the reflected shock wave, P_6 is the pressure behind a similar shock wave reflected from a rigid wall and P_2 is the pressure behind the incident shock wave. It is evident that during the interaction with a granular layer the incident shock wave is partially transmitted inside the layer and the reflected shock wave must be weaker than that for a similar shock wave reflection from a rigid wall. Thus, for a granular layer the interface coefficient C_R must be smaller than unity.

The propagation of the transmitted wave inside the layer depends not only on the area available to the gas flow, but also on the friction force F_G which according to [7], increases sharply across the interface. The role of the porosity and the particle diameter of the material can be taken into account if the porosity ϵ in [7] is replaced by the coefficient of permeability f. Using the Carman–Kozeny equation [1], [7] can be rewritten as:

$$\frac{F_G}{\epsilon_G} = -\left[\frac{\epsilon_G \mu V_G}{f} + \rho_G V_G^2 \sqrt{\frac{4}{45}\frac{\epsilon_G}{f}}\right], \quad \text{for} \quad \epsilon_G \neq 1. \qquad [14]$$

Equation [14] shows that the magnitude of the friction force during the transmitted wave propagation is directly related to the layer permeability, f. Therefore, it should be expected that the smaller the layer permeability is, the stronger is the reflected shock wave. This expectation is confirmed by the experimental and the numerical results shown in figure 3 for samples of different materials having a layer depth $L = 37 \pm 2$ mm. As can be seen from these data the coefficient C_R is a decreasing function of the layer permeability f.

In order to answer the question whether the maximum quasi steady pressure level P_e reaches the equilibrium value P_6 the experimental values of the coefficient C_E are also shown in figure 3. It is clear from this figure that the experimental results for P_e coincide with P_6 in the range of $P_6 \pm 3\%$ which does not exceed the 5% uncertainty for the pressure measurements. For a deeper layer, the equilibrium pressure behind the reflected shock wave during the test time period $\Delta T \approx 3$ ms is not reached.

In summary, two conclusions, concerning the discussed phenomenon can be drawn.

(1) The gas pressure measured before the gas–granular layer interface increases gradually from the initial pressure $P_R < P_6$ to an equilibrium pressure, $P_e \approx P_6$. The amplitude of the initial pressure jump decreases with the permeability of the granular layer.

(2) The flow field behind the reflected shock wave as observed in the experiments is correctly predicted by the simple filtration model which does not take into account the compaction effects and the porosity reduction associated with the transmitted wave propagation inside the sample. Close agreement between the experiments and the numerical simulations justified the suggestion

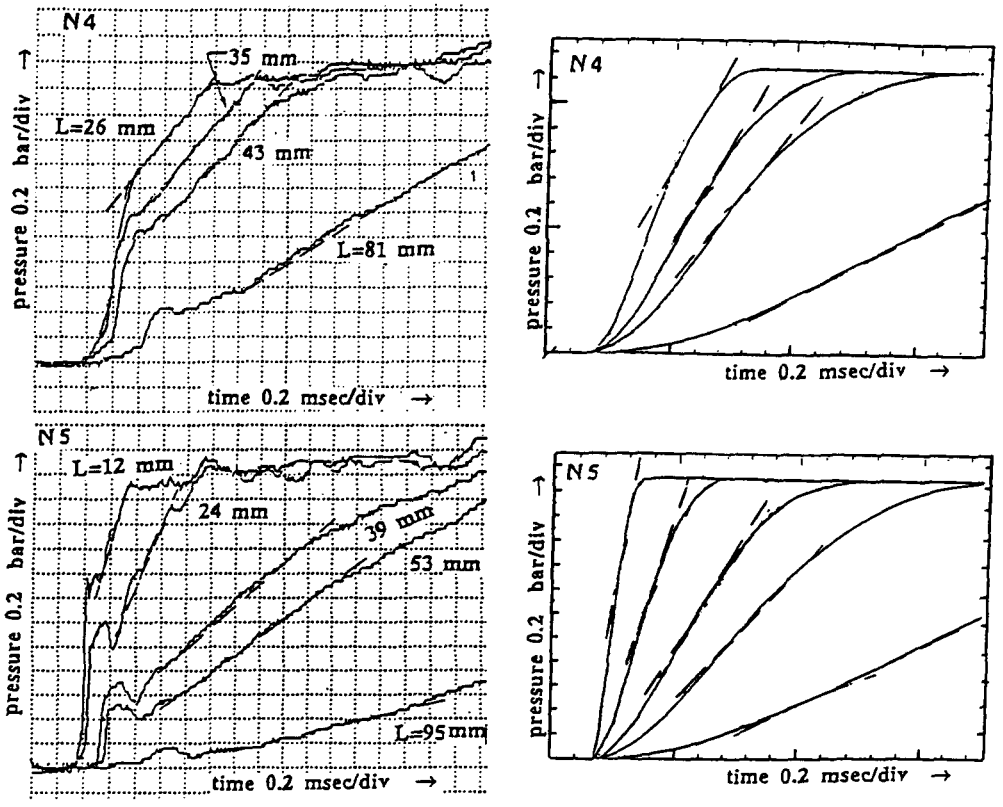

Figure 8. Typical gas pressure signals from transducer T4 (on the left) and their numerical simulation (on the right) for material N4 and N5 and different sample depths. Dotted straight lines show the tangent to the linear sections of the curves.

that the gas filtration through the layer is the main factor determining the pressure history ahead of the granular layer.

4.2. Gas filtration inside the granular layer

The role of the compaction wave during the gas filtration through the granular layer is still poorly understood. Basically, the problem stems from the fact that the gas entrapped in the compaction wave front can be strongly compressed and may increase its resistance to the gas flow (Britan *et al.* 1997). If the incident shock wave is weak, the effect of the granular layer compression is small and it is reasonable to suppose that the effect of the compaction wave on the gas filtration is also relatively weak. As was observed previously (see, e.g. Ben-Dor *et al.* 1997) the compressive stress attenuates in the granular layer and the magnitude of the effect of the compaction wave also changes with the granular layer depth. It can be also expected that the effect of the compaction wave on the gas pressure will decrease along the layer. Thus, after some distance the gas pressure inside the sample is determined by the filtration. Verifying the simple filtration model was the main reason for conducting experiments by which a comparison between the side-wall gas-pressure measurements at different locations and the model calculations could be made.

Another reason for such a comparison is related to the procedure of the pressure measurements at the side-wall in the granular media. It is well known, that the granular layer porosity increases in the vicinity of the confining walls (Goldshtik 1984). This phenomenon may result in multi-dimensional effects near the walls, and a question arises whether or not this gas flow affects the side-wall pressure.

In order to answer these questions the pressure traces from transducers T1, T2 and T3 are compared in figure 4 with the calculated pressure profiles for all the materials listed in table 1. The solid lines and the black points with the error bars represent mean pressure profiles based on results from 4–5 experiments and the dotted lines are the results of the corresponding numerical

simulations. Considering the repeatability and the experimental errors it is apparent that a good to excellent agreement exists between the calculated and the experimental pressure profiles. The good agreement which is observed for all the measuring positions along the sample and for all the materials under investigation is a surprise and seems to be in contradiction with the above predictions.

This good agreement confirms the dominant role of the gas filtration in the formation of the gas pressure in the sample. Moreover, it also shows that the difference in the material permeability near the side-wall and at the center of the sample have a negligibly small effect on the side-wall pressure measurements. The last but probably the most important point to emphasize is that the proposed one-dimensional model which does not account for the compression of the sample is suitable for describing the gas pressure at the side-wall. The question arises why the compression has no effect on the local gas pressure at least when the compaction wave passes the transducer.

The possible explanation of this behavior can be attributed to the dissipative characteristics of the granular medium. The data in figure 4 clearly indicate that the transmitted wave is more likely to be a compression fan which spreads out with time. The gaseous phase dissipates its energy and momentum in the course of the interaction with the solid phase and causes the formation of a compaction wave. However, the motion of the particles is promptly stopped by the bridging forces and the friction between the particles, and most of the momentum and the energy transferred to the solid phase are dissipated (Britan *et al.* 1997). Thus, as long as a good agreement between the theory and the experiments is obtained, the magnitudes of the energy and the momentum losses

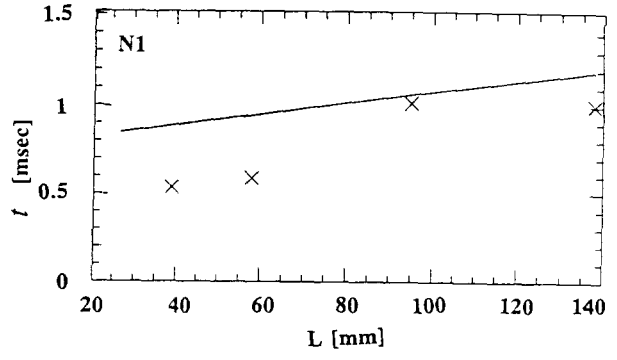

(a)

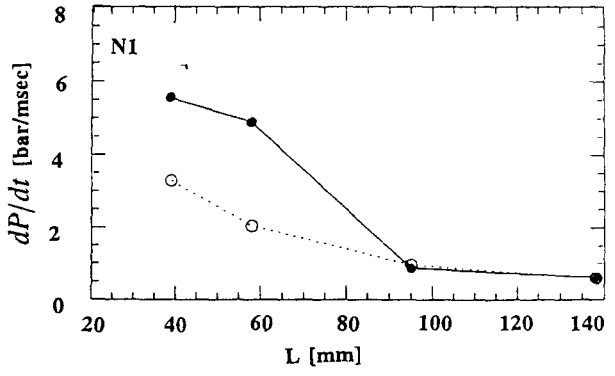

(b)

Figure 9. (a) Correlations between the time of the linear section origin of the signals from transducer T4 and the time of the maximum of the signals from transducer T5 vs the granular layer depth L. (b) Comparison between the calculated (open points) and the measured (black points) gas pressure rates for the linear part of the signals from transducer T4. Granular material N1.

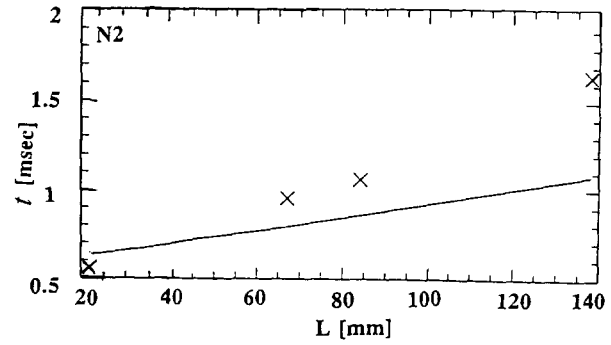

(a)

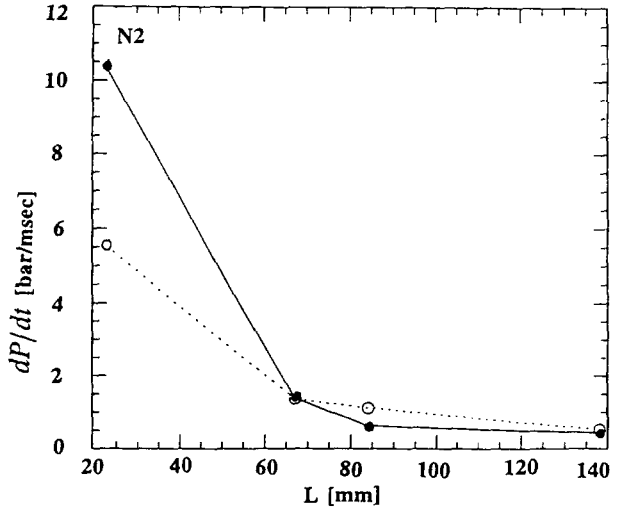

(b)

Figure 10. (a) Correlations between the time of the linear section origin of the signals from transducer T4 and the time of the maximum of the signals from transducer T5 vs the granular layer depth L. (b) Comparison between the calculated (open points) and the measured (black points) gas pressure rates for the linear part of the signals from transducer T4. Granular material N2.

in the gaseous phase in the experiments and the calculations, are the same, and the energy losses related to the compaction wave formation are small.

Contrary to the lateral effect, the longitudinal compression of the sample is more pronounced. Friction forces and arching inside the solid phase can not stop so quickly the motion of the particles and the formation of the compaction wave strongly increases the resistance of the layer to the gas flow in the downward direction (Britan *et al.* 1997).

In view of the above discussion the further analysis is concerned with the question whether the longitudinal compression of the sample affects the gas pressure measured at the shock tube end-wall. Some of the supporting evidence for the importance of this effect comes from recent shock tube experiments by Yasuhara *et al.* (1996) who investigated flexible foams. Notably, the end-wall gas pressure signals, shown in this paper, actually repeat, in some cases, profiles of the compressive stress signals measured at the end-wall. Thus, the end-wall and the side-wall gas pressure signals measured in the granular layer must be also different.

Bearing this in mind the calculated results are compared in figure 5 with the gas pressure signals measured by transducers T3 and T4. In the experiments transducer T3 (see figure 1) is located at the side-wall 18 mm from transducer T4 which is flush mounted on the end-wall. The difference in their signals can provide an indication of the existence of longitudinal pressure gradients in this area. Gas pressure signals (obtained with two samples of different depths and materials) were used

to elucidate the effect of the granular layer depth and permeability on the formation of the gas pressure profile.

During the test time the gas pressure inside the large permeability material N2 reaches the equilibrium value $P_e \approx 2.3$ bar whereas inside the long sample with small permeability material N4 it only reaches half of this value. Approximately the same tendency is observed in the numerical calculations. The results of the side-wall measurements are quite different from those measured at the end-wall, especially when the permeability of the sample is small. Notably, the gas pressure histories are smooth and do not show evidence of the existence of sharp front variations in amplitude which might correspond to the arrival of the compaction wave reflected from the end-wall. This behavior is unusual since the gas flow conditions must affect at least the signal from transducer T3 which is positioned close to the end-wall. Moreover, if the pressure fluctuations related to the unsteady conditions at the end-wall had propagated away from the rear-end of the layer, the calculated and the experimental results for the side-wall measurements would not agree. However, in contrast to this hypothesis all the side-wall pressure signals agree quite well with the calculations.

As can be seen in figure 5 after a slowly rising precursor in the signals measured by transducer T4 a sharp pressure rise, which is more than twice larger than that measured at the same time by the transducer T3, appears. After this sharp increase the pressure increases gradually. Notably, the unsteady spike in the signals is not reproduced by the simple filtration model, and there are reasons to believe that it is related to the influence of the compaction wave on the end-wall gas pressure.

4.3. *Effect of the compaction wave on the end-wall gas pressure*

In order to demonstrate the correlation between the gas pressure and the compressive stress profiles measured at the end-wall, the signals from transducers T4 and T5 are reproduced in figure 6 along with the wave diagrams obtained previously with the samples of depth $L = 138$ mm (see, e.g. Ben-Dor *et al.* 1997). In the context of this study the data in figure 6 provide the basis for the explanation of the role of the compaction wave in the gas pressure formation at the end-wall. The gas pressure signals from transducers T4 and T5 were obtained in the experiments with the end-wall positioned at the measuring points shown in the wave diagrams by the arrows (A:) and (B:).

After the gas near the end-wall is compressed by the transmitted wave, the compaction wave compresses it to the higher pressure and stops the motion of the particles. Since the compaction wave originates inside the sample as a thin piston-like region of compressed particles, after reflection at the end-wall it can isolate gas near the end-wall from that inside the granular layer (see, e.g. Britan *et al.* 1997). The discrepancy between the measured and the calculated gas pressure signals as shown in figure 5 depends ultimately on whether or not gas flows through the compaction wave front. The permeability of the compaction wave to the gas at a later time, after the reflection at the end-wall, can be related to the destructive pressure gradients which drive the hot gas back from the end-wall (Skews *et al.* 1993). Clearly, such a complicated phenomenon deserves further study.

The results presented in figure 6 indicate that the variations in the layer permeability result in different flow patterns inside the layer and in different pressure signals. For the material N2 (whose permeability coefficient is about $f \approx 0.005$ mm^2, see table 1) the trajectories of the transmitted wave (dotted line) and the compaction wave (solid line) are straight lines and they all originate at the origin $x = 0$. The arrival of the transmitted wave at the location (A:) is safely registered by transducers T4 and T5 as a sharp jump followed by a gradual pressure increase which depends on the filtration of the gas flow induced by the transmitted wave. Both of these transducers register similar pressure profiles terminated by a strong spike in the signal from transducer T5 which is most probably a result of the compaction wave arrival at the end-wall. Two remarks, which are of particularly importance for understanding this phenomenon, must be made.

During the impact the particles do not move immediately behind the transmitted wave. The time delay which is observed in the signals of figure 6 between the moment of the transmitted wave reflection at the end-wall and the compaction wave arrival is indicative of the inertia of the granular layer.

The signals from transducer T5 show the history of the compressive stress which depends on the variation in the granular layer porosity in the vicinity of the end-wall. The compressive stress signal is maximal when the porosity of the sample near the end-wall approaches the minimum value. After the maximum, the compressive stress signal decreases but the porosity increases until the signals from transducers T4 and T5 register the same equilibrium pressure $P_e \approx P_5$ (Ben-Dor *et al.* 1997; Britan *et al.* 1997).

Contrary to the later case, the signals obtained at location (B:) do not reach equilibrium immediately after the unsteady spike but only increase gradually. The initial profile of the gas pressure resembles a spike in the compressive stress measured by transducer T5. In addition, the time delay in the compaction wave arrival at the end-wall is more pronounced. Since the gas filtration is the main process providing pressure equalization inside samples of large permeability, it can be concluded that the filtration rate decreases with the granular layer depth whereas the effect of the compaction wave on the end-wall pressure increases.

At the same time the signals from transducers T4 and T5 obtained for material N4 (for which $f \approx 0.0002$ mm^2) show a precursor before the transmitted wave even at the location (A:). According to the wave diagram for this material the transmitted and the compaction waves propagate along the layer with nearly the same velocities and close to the location (B:) they interact. Thus, the time delay between the transmitted and the compaction waves arrival at location (B:) is extremely small.

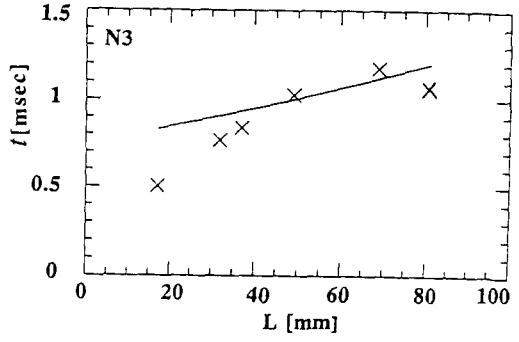

(a)

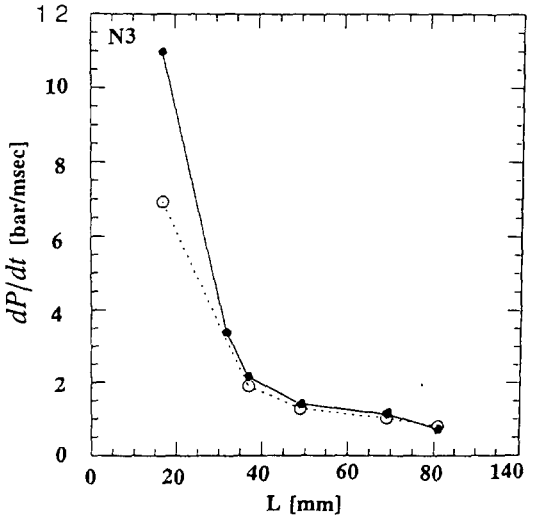

(b)

Figure 11. (a) Correlations between the time of the linear section origin of the signals from transducer T4 and the time of the maximum of the signals from transducer T5 vs the granular layer depth L. (b) Comparison between the calculated (open points) and the measured (black points) gas pressure rates for the linear part of the signals from transducer T4. Granular material N3.

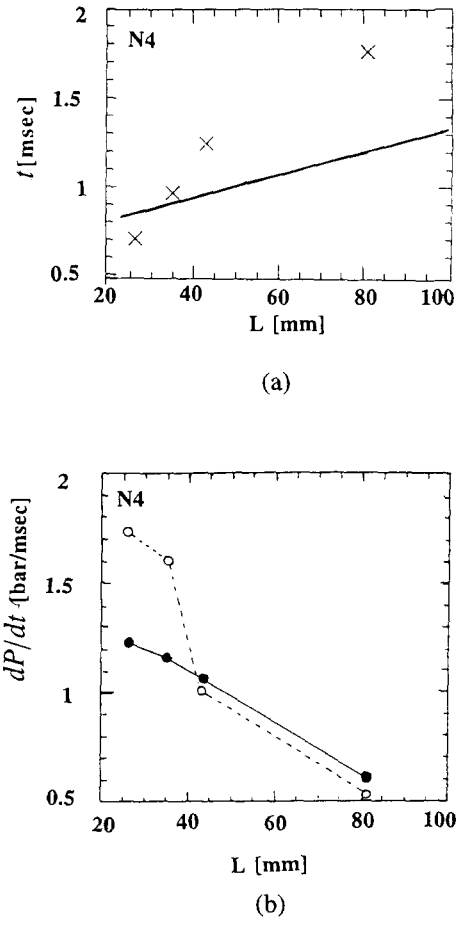

Figure 12. (a) Correlations between the time of the linear section origin of the signals from transducer T4 and the time of the maximum of the signals from transducer T5 vs the granular layer depth L. (b) Comparison between the calculated (open points) and the measured (black points) gas pressure rates for the linear part of the signals from transducer T4. Granular material N4.

The same tendency is observed in the pressure signals: a sharp rise in the gas pressure which manifests the moment of the compaction wave arrival is observed close to the moment of reflection of the transmitted wave from the end-wall.

In order to interpret the pressure/time signals measured by transducer T4 they are compared in figures 7 and 8 with calculations for the different sample depths and materials. The experimental signals are shown in the left side and the calculations are shown in the right side of these figures. As expected, the general trend is that the profile of the signals changes significantly with the sample depth L.

The formation of the compaction wave inside the sample complicates the comparison between the measured and the calculated results because it affects the gas pressure signal during the whole test time from the beginning to the later part of the signals when the compaction wave has already disappeared. This contribution is called in the present study as a 'residual' effect since it makes the signals measured by transducer T4 to be higher than the calculated ones (see figure 6). This effect for the materials under investigation was discussed previously by Britan *et al.* (1997). Without going into detail we can use the data in figures 7 and 8 to elucidate the role of the gas filtration during the impact.

Inspection of figures 7 and 8 shows that the experimental signals consist of two important parts. Initial unsteady variations of the amplitude which are closely related to the compaction wave arrival at the end-wall and are most pronounced in the signals obtained with materials N2, N4 and N5. In the signals obtained with materials N1 and N3 these initial variations of the gas pressure are smoother. Comparison of the materials characteristics listed in table 1 and the calculated gas

pressure profiles shown in figures 7 and 8 gives no way of explaining the reasons for such a difference in the initial gas pressure profiles. One can use for this purpose the particle response time, $\tau_p = \rho_p d_p^2/18\mu$ (Britan *et al.* 1997). As expected, the maximum values of τ_p for materials N2, N4 and N5 is $\tau_p = 8.5$ s, while for material N1, $\tau_p = 50$ s and for material N3, $\tau_p = 26$ s. Thus the effect of the compaction wave on the end-wall gas pressure is stronger for the materials having smaller values of τ_p.

The second part of the signals measured at the end-wall demonstrates the continuous, almost linear increase of the gas pressure in the course of the gas filtration. It can be compared in its slope (i.e. the rate of the pressure increase) with the calculated one. If these two slopes are similar it can be suggested that the experimental and the simulated conditions for the gas filtration are the same. The data in figures 7 and 8 clearly show that the time duration of the linear part of the signals increases significantly with the granular layer depth L. For the deep layers, due to the small velocity of the filtration, this time is long but for the short layers it is shorter than the test time of the shock tube $\Delta T \approx 3$ ms.

The above procedure of comparing the calculated and the measured results enables us to avoid the residual effect but leaves open the question how to choose the linear part of the pressure signals. To answer this question straight dashed lines which were drawn as tangents to the curves with the origin at the location were gas pressures for the calculated and the experimental signals are the same, are shown in figures 7 and 8. Clearly, if the agreement between the experiment and the theory in the gas pressure increase rate is observed, the origin of the linear part specifies at the moment after which the role of the compaction wave becomes negligible and the gas pressure signal is determined by the gas filtration.

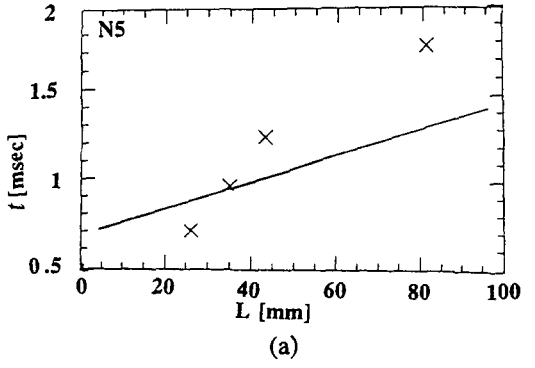

(a)

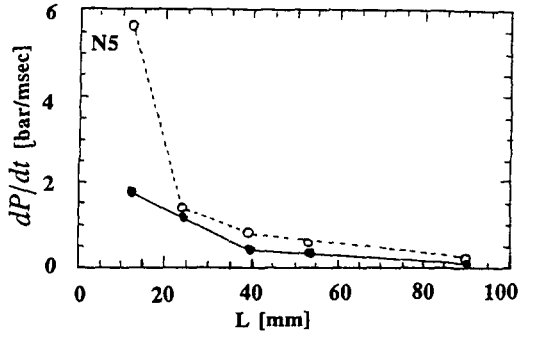

(b)

Figure 13. (a) Correlations between the time of the linear section origin of the signals from transducer T4 and the time of the maximum of the signals from transducer T5 vs granular layer depth L. (b) Comparison between the calculated (open points) and the measured (black points) gas pressure rates for the linear part of the signals from transducer T4. Granular material N5.

To ensure this one can refer to the data in figures 9–13. Curves (a) in these figures show the correlation between the instance of the linear part origin in the experimental signals in figures 7 and 8 (cross points) and the time of the maximum in the compressive stress signals (solid lines). As discussed previously, the maximum in the compressive stress agrees quite well with the maximum effect of the compaction wave on the end-wall gas pressure (Britan *et al.* 1997). Curves (b) in these figures demonstrate the calculated (open) points and measured (black points) gas pressure increase rates obtained for the same conditions. Analysis of these data leads to the following conclusions:

(1) There exists an initial depth of the layer $L < L^*$, for which regardless of the material characteristics, the compaction wave compresses the gas in the vicinity of the end-wall ('piston' effect). Due to the piston effect a difference is observed in the measured and the calculated pressure increase rates for these conditions.

(2) For longer layers $L > L^*$, the end-wall conditions for most part of the test time are dominated by filtration because the compaction wave attenuates inside the layer, and the piston effect is weak. Clearly, in this case close agreement is observed between the measured and the calculated pressure increase rates.

(3) Any attempt to choose the linear part within the initial unsteady period of the gas pressure signal, closer to the maximum of the compressive stress, results in a difference between the measured and the calculated pressure increase rates. On the other hand, if the linear part begins after the time when the maximum of the compressive stress is attained, the calculated and the experimental gas pressure increase rates agree quite well for all the investigated materials and layer depths.

5. CONCLUSIONS

The gas filtration through five types of granular layers during weak shock wave impact were investigated experimentally and numerically. The purpose was to study the behavior of the gas pressure at the side-wall above and inside the layer and the dynamics of the gas pressure formation at the end-wall.

It was found that the side-wall pressure traces above the layer show an initial pressure jump, which is followed by a gradual pressure increase to an equilibrium pressure corresponding to the incident shock wave reflection from a rigid wall. The amplitude of the initial pressure jump decreased with the permeability of the granular layer.

Side-wall pressure traces inside the layers have a smooth profile without any evidence of the existence of sharp front variations in the amplitude which might correspond to the arrival of the reflected waves from the end-wall,

The gas pressure traces obtained at the end-wall consist of two parts: initial unsteady variations of the amplitude which are closely related to the effect of the compaction wave on the gas pressure, and a continuous, approximately linear part when the gas pressure increases in the course of the gas filtration.

The mass, momentum and energy conservation equations, describing compressible one-dimensional gas flow in a granular layer were presented. The developed model employed a homogeneous mixture approximation and neglected the porosity changes in the granular layer. The momentum and energy transfer rates between the granular medium and the gas were calculated using the phenomenological correlations for packed beds. These equations were solved numerically using a TVD numerical scheme. Contrary to the most known studies in this field no adjustable parameters were used in the calculations.

Good agreement is found between the calculations and the side-wall pressure measurement above the granular layer. For the later stage of the experimental gas pressure signals good agreement is observed with the calculated pressure increase rates when the end-wall conditions are governed by gas filtration. In the initial unsteady part of the signals large discrepancies exist between the calculations and the experiments due to the effect of the compaction wave on the gas pressure. Based on this experimental evidence the physical processes which are responsible for this behavior are discussed. To the best of our knowledge such a comparison of the experimental results obtained at the end-wall covered by different materials and for various layer depths has not been performed in previous studies on weak shock wave impact with granular layers.

A good to excellent agreement between the experimental results and the calculations is also found for the side-wall gas pressure signals obtained inside the granular layers. The reasons for this behavior are not well understood as yet. If this behavior is not a result of the gas flow leakage through the gap between the side-wall and the granular layer it can be concluded that the lateral effects of the compaction wave on the gas pressure in these experiments are bound to be negligible, and the suggested one-dimensional model is well suited also for predicting the gas pressure at the side-wall.

Acknowledgements—The authors are grateful to Mr Doron Goder for his assistance in conducting the measurements of the materials characteristics. This study was supported by the Israeli Ministry of Science and Art under Grant # 4094-1-92.

REFERENCES

Ben-Dor, G., Levy, A. and Sorek, S. (1996) Simulations of waves propagation in saturated rigid porous media and comparisons with experiments. *Proceeding of the Asia-Pacific Conference on Shock & Impact Loads on Structures*, Singapore, January, pp. 25–32.

Ben-Dor, G., Britan, A., Elperin, T., Igra, O. and Jiang, J. P. (1997) Experimental investigation of the interaction between weak shock waves and granular layers. *Exp. Fluids* (to appear).

Bird, R. B., Stewart, W. E. and Lightfoot, E. N. (1960) *Transport Phenomena*. J. Wiley, New York.

Britan, A., Elperin, T., Igra, O. and Jiang, J. P. (1995) Head-on collision of a planar shock wave with a granular layer. *Proceedings of the ISCCM Conf.*, eds S. C. Schmidt and W. C. Tao, Part 2, pp. 971–974, Seattle, WA.

Britan, A., Ben-Dor, G., Elperin, T., Igra, O. and Jiang, J. P. (1997) Mechanism of compressive stress formation during weak shock waves impact with granular materials. *Exp. Fluids* (to appear).

Drew, D. A. (1983) Mathematical modeling of two-phase flow. *Annual Review of Fluid Mechanics* **15,** 261–291.

Dullien, F. A. (1992) *Porous Media*. Academic Press, New York.

Gelfand, B. E., Medvedev, S. P., Borisov, A. A., Polenov, A. N., Frolov, S. M. and Tsyganov, S. A. (1989) Shock loading of stratified dusty system. *Combustion* **9,** 153–165.

Goldshtik, M. A. (1984) Transfer processes in granular layer. Academy of Sciences of the USSR, Siberian Branch, Institute of Thermophysics, Novosibirsk.

Gouph, P. S. and Zwarts, F. J. (1979) Modeling heterogeneous two-phase reaction flow. *AIAA Journal* **17,** 17–25.

Hirsch, C. (1991) *Numerical Computation of Internal and External Flows*, Vols 1 and 2. J. Wiley, New York.

Ishii, M (1975) *Thermo-fluid Dynamic Theory of Two-phase Flow*. Eyrolles, Paris.

Kaviany, M. (1991) *Principles of Heat Transfer in Porous Media*. Springer, New York.

Kutushev, A. G. and Rudakov, D. A. (1993) Numerical study of the action of a shock wave on an obstacle screened by a layer of porous powder materials. *Comb. Expl. Shock Waves* **5,** 25–31.

Levy, A., Ben-Dor, G., Skews, B. W. and Sorek, S. (1993) Head-on collision of normal shock waves with rigid porous material. *Exp. Fluids* **15,** 183–190.

MacDonald, I. F., El-Sayed, M. S. and Dullien, F. A. (1979) Flow through porous media — the Ergun equation revisited. *Ind. Eng. Chem. Fundam.* **18,**.

Molerus, O. (1993) *Principles of Flow in Disperse Systems*. Chapman and Hall, London.

Rogg, B., Hermann, D. and Adomeit, G. (1985) Shock-induced flow in regular arrays of cylinders and packed beds. *Int. J. Heat and Mass Transfer.* **28,** 2285–2297.

Sakakita, H. and Hayashi, K. (1992) Study on interaction between a powder layer and a shock wave. *18th Int. Symp. Shock Waves*, Kagoshima, Japan.

Skews, B. W., Atkins, M. D. and Seitz, M. W. (1993) The impact of a shock wave on porous compressible foams. *J. Fluid Mech.* **253,** 245–265.

Yasuhara, M., Watanabe, S., Kitagawa, K., Yasue, T. and Mizutani, M. (1996) Experiment on effects of porosity in the interaction of shock wave and foam. *Int. J. JSME, Ser. B* **39,** 287–293.